ADVANCES IN ATMOSPHERIC SCIENCES, VOL. 23, NO. 4, 2006, 521–530

Air-sea Interaction of Typhoon Sinlaku (2002) Simulated by the Canadian MC2 Model

REN Xuejuan*[1] (任雪娟) and William PERRIE[2]

[1] *Department of Atmospheric Sciences, Nanjing University, Nanjing* 210093

[2] *Bedford Institute of Oceanography, P. O. Box 1006, Dartmouth, NS, B2Y 4A2, Canada*

(Received 15 April 2005; revised 9 September 2005)

ABSTRACT

Three experiments for the simulation of typhoon Sinlaku (2002) over the western North Pacific are performed in this study by using the Canadian Mesoscale Compressible Community (MC2) atmospheric model. The objective of these simulations is to investigate the air-sea interaction during extreme weather conditions, and to determine the sensitivity of the typhoon evolution to the sea surface temperature (SST) cooling induced by the typhoon. It is shown from the three experiments that the surface heat fluxes have a substantial influence on the slow-moving cyclone over its lifetime. When the SST in the East China coastal ocean becomes 1°C cooler in the simulation, less latent heat and sensible heat fluxes from the underlying ocean to the cyclone tend to reduce the typhoon intensity. The cyclone is weakened by 7 hPa at the time of its peak intensity. The SST cooling also has impacts on the vertical structure of the typhoon by weakening the warm core and drying the eye wall. With a finer horizontal resolution of $(1/6)^\circ \times (1/6)^\circ$, the model produces higher surface wind, and therefore more surface heat fluxes are emitted from the ocean surface to the cyclone, in the finer-resolution MC2 grid compared with the relatively lower resolution of $0.25^\circ \times 0.25^\circ$ MC2 grid.

Key words: typhoon, air-sea interaction, SST cooling, MC2

doi: 10.1007/s00376-006-0521-4

1. Introduction

Tropical cyclones develop over the data-sparse tropical oceans. They are a serious type of natural disaster both because of the loss of human life they cause and the large economic losses they induce. Tropical cyclones derive energy primarily from evaporation from the ocean and the associated condensation in convective clouds concentrated near their centre (Holland, 1993). The warm-core structure within a tropical cyclone produces very strong surface winds and causes damage to coastal regions through high-speed wind, huge storm surges and waves, and heavy rain. Although great progress has been achieved in tropical cyclone simulation in the last forty years, it is still a challenge to accurately simulate tropical cyclone formation, intensification and storm track (Masashi et al., 2001; Meng et al., 2002). Emanuel (1999) demonstrated that the evolution of hurricane intensity depends mainly on three factors: the storm's initial intensity, the thermodynamic state of the atmosphere through which it moves, and the upper ocean properties along the storm track. The momentum and enthalpy exchanges at the air-sea interface accompanying the passage of a cyclone are the dominant processes between the tropical cyclone and the ocean underlying. The surface heat fluxes increase the buoyancy of the air in the boundary layer, and latent heat is released in the frontal cloud later. The cyclone intensity can be strongly modulated by pre-existing oceanic features, such as a warm-core eddies or sea surface temperature (SST) cooling induced by a previous cyclones (Bao et al., 2000). On the other hand, a slow moving cyclone can generate crescent-shaped SST cooling within one or two days, which can be clearly detected in a satellite images (Wentz et al., 2000), and results from cyclone-induced entrainment mixing at the bottom of the oceanic mixing layer (Ren et al., 2004; Perrie et al., 2004). The SST cooling reduces the sea surface heat fluxes, which subsequently leads to reduced storm intensity. (Bender and Ginis, 2000; Bao et al., 2000; Perrie et al., 2004).

On the average, 26 tropical cyclones occur over the western North Pacific per year, with the maximum cy-

*E-mail: renxuej@nju.edu.cn

clone activity in August and a high degree of seasonal variation. This total is more than that in any other region (Xue and Neumann, 1984). About 7 or 8 typhoons making landfall in China per year, on average. In 2002, 5 tropical cyclones made landed in Mainland China (Mekkhala, Hagupit, Sinlaku, Vongfong, and Kammuri). Sinlaku had the strongest wind at landfall, compared to the other four landfalling typhoons (Lu, 2003). The purpose of this study is to investigate the role of air-sea fluxes on the evolution and vertical structure of typhoon Sinlaku. We consider simulations of typhoon Sinlaku over the western North Pacific Ocean, using the well-tested Canadian Mesoscale Compressible Community (MC2) atmospheric model. A brief description of the atmospheric model used in this study is presented in section 2. The typhoon case and the experimental design are also described there. Numerical results of the typhoon simulations are discussed in section 3 with consideration of the impact of air-sea interaction on typhoon evolution. Conclusions are given in section 4.

2. Model description, typhoon case introduction and experimental design

2.1 *Model description*

Robert et al. (1985) originally developed the MC2 atmospheric model used in this study. It has evolved as a result of cooperative research involving scientists from universities and the Meteorological Service of Canada (MSC). The model is described in http://collaboration.cmc.ec.gc.ca/science/rpn.comm/. It is a state-of-the-art fully elastic nonhydrostatic model solving the full Euler equations on a limited-area Cartesian domain. MC2 uses semi-Lagranigan advection and a semi-implicit time-differencing dynamic scheme. This model has proven to be quite versatile as a modeling tool, allowing excellent simulations over a wide spectrum of scales (Benoit et al., 1997). It has also been used to successfully simulate Northwest Atlantic cyclones (McTaggart-Cowan et al., 2001, 2003) and western North Pacific typhoons (Li., 2004). Further details on the model dynamics are given by Benoit et al. (1997).

The model is implemented on the domain of 10.0°N to 44.5°N and 107.5°E to 147.0°E and with a horizontal resolution of 0.25° × 0.25° and 30 vertical layers, using latitude-longitude projection. The integration time step is 600 s. Initial conditions, lateral boundary conditions, and SST are determined from the analysis data generated by the regional data assimilation system at the Canadian Meteorological Centre (CMC) as described by Chouinard et al. (1994). The MC2 model interpolates linearly in time between analyses to obtain boundary conditions for every time step. A force-restore scheme, described by Benoit et al. (1997), is used to calculate surface heat and moisture fluxes over land. The surface fluxes above the sea are calculated using Monin-Obukhov similarity theory. Deep cumulus convection is parameterized using the Kain-Fritsch scheme (Kain and Fritsch, 1990, 1993).

2.2 *Typhoon case*

Typhoon Sinlaku began its extended lifecycle as a tropical depression at 16.7°N, 154.3°E at 1800 UTC 28 August 2002 and became tropical storm twelve hours later. Sinlaku became a typhoon near 22.5°N, 152.6°E at 1200 UTC 30 August and developed maximum sustained winds of 110 knots. The system turned more westward by the end of the month, passing west of 135°E near 25°N early on 3 September. Sinlaku's storm track during 4–7 September is shown in Fig. 1, as reported by the JTWC (Joint Typhoon Warning Centre, http://metoc.npmoc.navy.mil/jtwc.html). Sinlaku crossed the Japanese island of Okinawa on 4 September with maximum sustained winds of 95 knots. Subsequently, the typhoon headed towards Taiwan, carrying sustained winds of 90 knots. After tearing through the Okinawa island chain and Taiwan, Typhoon Sinlaku slammed into Mainland China. It tracked into Zhejiang province at noon on 7 September, making landfall near the city of Wenzhou. During 4 September, Sinlaku moved slowly with a displacement speed of about 5 m s^{-1}. During 5–6 September, it decelerated as it propagated over the coastal ocean, with a speed of less than 2.5 m s^{-1}. Previous idealised

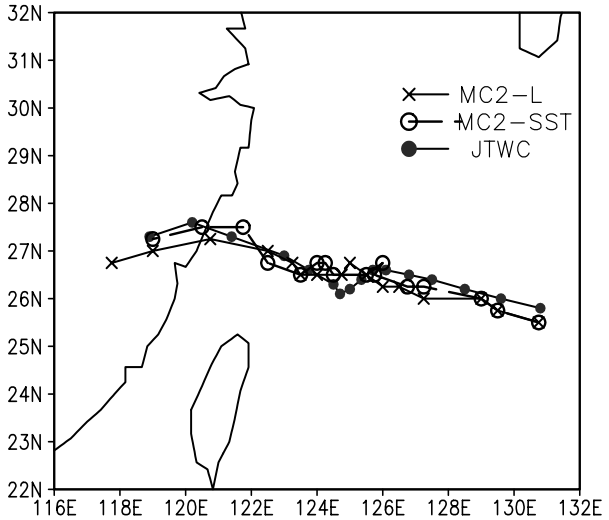

Fig. 1. Comparisons between the MC2-L track (crosses) simulation, with the MC2-SST simulation (open circles) and the JTWC-reported storm track (closed circles). The integration is from 0000 UTC 4 September to 1800 UTC 7 September, with the 6-hour interval indicated.

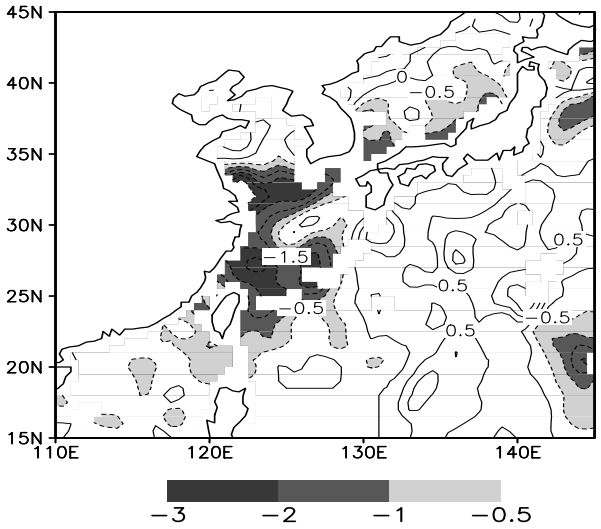

Fig. 2. SST difference during the passage of typhoon Sinlaku (7 September minus 31 August). SST data is from the 50 km Sea Surface Temperature Global dataset (SST50) from NOAA http://www.saa.noaa.gov/. It is a composite gridded-image derived from 8-km resolution global SST Observations and is generated twice weekly (Tuesday and Saturday) on a global scale by NOAA. The contour interval is 0.5°C.

and real case studies show that slow-displacement typhoons, with a shallow ocean mixed layer depths, can produce SST cooling along their storm tracks (Bender and Ginis, 2000; Chan et al., 2001). This is also reflected in the satellite data of Sinlaku. As shown in Fig. 2, during the passage of Sinlaku, an obvious SST cooling area extends from south to north along China's eastern coastal waters, with the maximum SST cooling of −3.4°C located between the Yellow Sea and the East China Sea.

2.3 *Experimental design*

All of the experiments are listed in Table 1. The control run, denoted MC2-L, is carried out with the MC2 model with a horizontal resolution of 0.25° × 0.25° and the model domain described above, using CMC analysis data to provide initial and lateral boundary conditions, as well as the SST field at the initial time (0000 UTC 4 September). The SST field in MC2-L is time-invariant during the whole integration period. The sensitivity experiment denoted MC2-SST is performed in manner as the simulation MC2-L, but with 1°C reduction in SST in the coastal water region of 24°N–34°N, 120°E–130°E. The reduced SST region is chosen according to Fig. 2. According to Zhang and Wang (2003), changing the vertical resolution has significant effects on hurricane intensity and structure. In order to investigate the influence of model resolution on the typhoon simulation, especially on air-sea heat fluxes, a third sensitivity experiment denoted MC2-H is performed using a finer horizontal resolution of (1/6)° × (1/6)°, with a domain of 17°N–37°N, 113.5°E–137°E. The three experiments are integrated from 0000 UTC 4 September to 1800 UTC 7 September 2002.

Table 1. List of experiments conducted.

Experiment name	Description
MC2-L	Simulations by 0.25° × 0.25° MC2 model, with time-invariant SST
MC2-SST	Same as MC2-L but for 1°C reduction of SST in the region of 24°–34°N, 120°–130°E, during the whole integration time
MC2-H	Same as MC2-L, but for a finer resolution of (1/6)° × (1/6)°, with the domain of 17°–37°N, 113.5°–136°E.

3. Simulation results

3.1 *Overview of the simulated typhoon results*

The evolutions of minimum sea level pressure (MSLP) and maximum surface wind speed ($V_{\max}$) of Sinlaku from the JTWC and the three experiments are plotted in Figs. 3a and 3b, respectively. The large differences between the JTWC and the simulations at the initial time in the figures are because of the weak initial vortex in the CMC analysis data. In other studies, the initial vortex provided by the large-scale analysis data is often too weak, and sometimes misplaced (Zou and Xiao, 2000). Many successful simulations, including prediction of cyclone intensity and track, were carried out by implanting a bogus vortex into the large-scale analysis of the initial state (Lord, 1991; Kurihara et al., 1993). There is no bogus vortex in the three experiments in the present study, because the bogus technology for improved typhoon simulation is not the focus of this paper. The reader is directed to Zou and Xiao (2000) for more details concerning the bogus data assimilation scheme.

The spin up of the simulation is quite fast. For example, within 18 hours, the MSLP simulated by MC2-L drops from 991 hPa to 980 hPa with $V_{\max}$ increasing from 19 m s^{-1} to 26 m s^{-1}. The simulated typhoon in MC2-L reaches its peak MSLP and $V_{\max}$ at 1800 UTC 6 September and 0400 UTC 6 September, respectively, with the values of 961 hPa for MSLP and 31 m s^{-1}

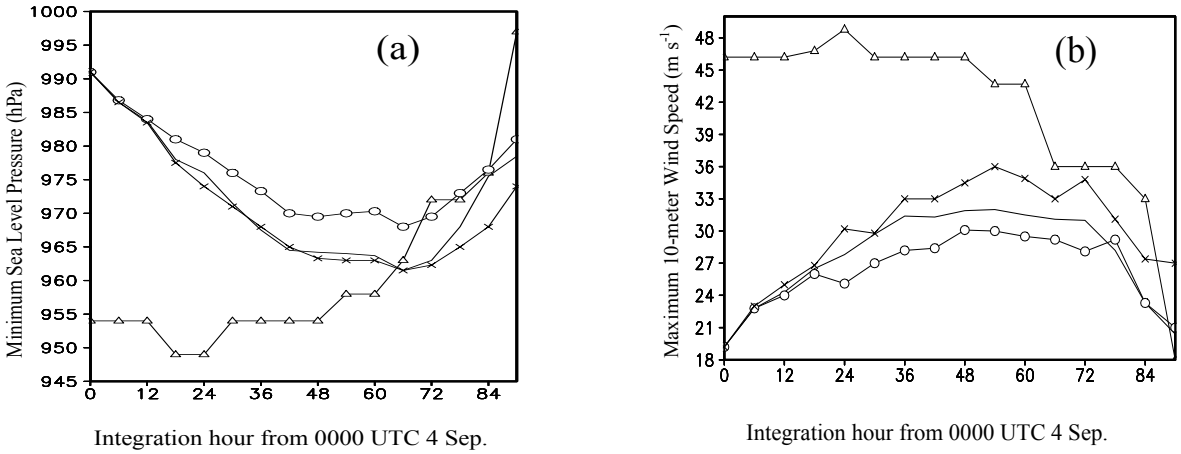

Fig. 3. Time series of (a) minimum sea level pressure (MSLP) in hPa, (b) maximum 10-m wind ($V_{\max}$) in m s^{-1}, for MC2-L (line), MC2-SST (open circles), MC2-H (crosses), and JTWC (triangles).

for $V_{\max}$. The simulated typhoon weaken rapidly after the peak intensities in the three experiments, in agreement with the JTWC analysis. The MSLP difference between MC2-L and MC2-SST becomes obvious after 12 h of integration in Fig. 3a. The cyclone is weaker in MC2-SST, which has SST cooling. The biggest difference in MSLP between MC2-SST and MC2-L is 7 hPa at 1800 UTC 6 September. The $V_{\max}$ is also lower in MC2-SST than in MC2-L. The biggest difference in $V_{\max}$ between MC2-SST and MC2-L is -4 m s^{-1} at 0000 UTC 7 September. Compared with MC2-L, more accurate typhoon intensity is presented by MC2-SST during the typhoon's landfall. There is no obvious MSLP difference between MC2-H and MC2-L before landfall. With finer resolution, MC2-H produces higher $V_{\max}$ than MC2-L. For example, the $V_{\max}$ difference between MC2-H and MC2-L at the time of the peak wind of MC2-H is 5 m s^{-1}.

Comparisons between the JTWC, MC2-L and MC2-SST storm tracks are shown in Fig. 1. The MC2-H track is similar to that of MC2-SST, and therefore it is not shown in the figure. Slight initial differences at 0000 UTC 4 September result from analysis discrepancies between the JTWC and CMC analysis low positions. Thereafter, the typhoon propagation tracks in the simulations are similar to the JTWC results before 7 September. The typhoon in MC2-L moves faster after 7 September as it approaches landfall, and finally goes more inland than the JTWC analysis. Meanwhile, MC2-SST and MC2-H present similar tracks as that of the JTWC analysis, especially when approaching landfall and after.

3.2 *Horizontal distribution of surface wind field*

The blended winds, combining QuikSCAT and National Centers for Environmental Prediction analysis wind fields (QUIKSCAT/NCEP), available from http://www.ssmi.com/qscat/scatterometer_data_daily.html, depicts a well-organized circular wind field around the central eye region at 2100 UTC 6 September (see Fig. 4a). The wind speed around the eye is greater than 15 m s^{-1}. The maximum wind speed (>40 m s^{-1}) occurs in the southeast quadrant of the cyclone. The simulation results for 10-m wind fields from the three experiments are shown in Figs. 4b–4d, respectively. They present a well-defined and asymmetric wind structure converging cyclonically towards the bigger eyes. Compared with Fig. 4a, the model produces lower surface maximum wind. All of the maximum wind speeds in the three experiments are less than 35 m s^{-1}. With finer resolution, MC2-H represents clearly the high-speed wind belt with a maximum value of 33 m s^{-1} in the southeast quadrant of the cyclone.

3.3 *Vertical cross section*

Figure 5 depicts the vertical distributions of relative humidity and air temperature along the east-west oriented line through the eye of Sinlaku at integration hour 48 for the three experiments. The eye extends up to 200 hPa and has a radius of about 50 km. The relative humidity is more than 95% in the eye wall, from the surface to the middle troposphere. The eye is relatively dry in the troposphere, with relative humidity about 80% in the low level and 20% in the upper level. The warm core structure from the surface to 400 hPa in the eye is obvious. There are some differences between Fig. 5a (MC2-L) and Fig. 5b (MC2-SST). The warm core in the boundary layer in MC2-SST is weaker than that in MC2-L. For example, the air temperature at 900 hPa in the eye in MC2-SST is about 2.5°C lower than that in MC2-L. The eye wall is slightly dryer in the middle and upper troposphere in MC2-SST than in MC2-L. When the model horizontal resolution increases from $0.25° \times 0.25°$ to $(1/6)° \times (1/6)°$, the simulation MC2-H presents a narrower and a more complicated eye wall than MC2-L or MC2-SST.

Similar cross sections for potential temperature are

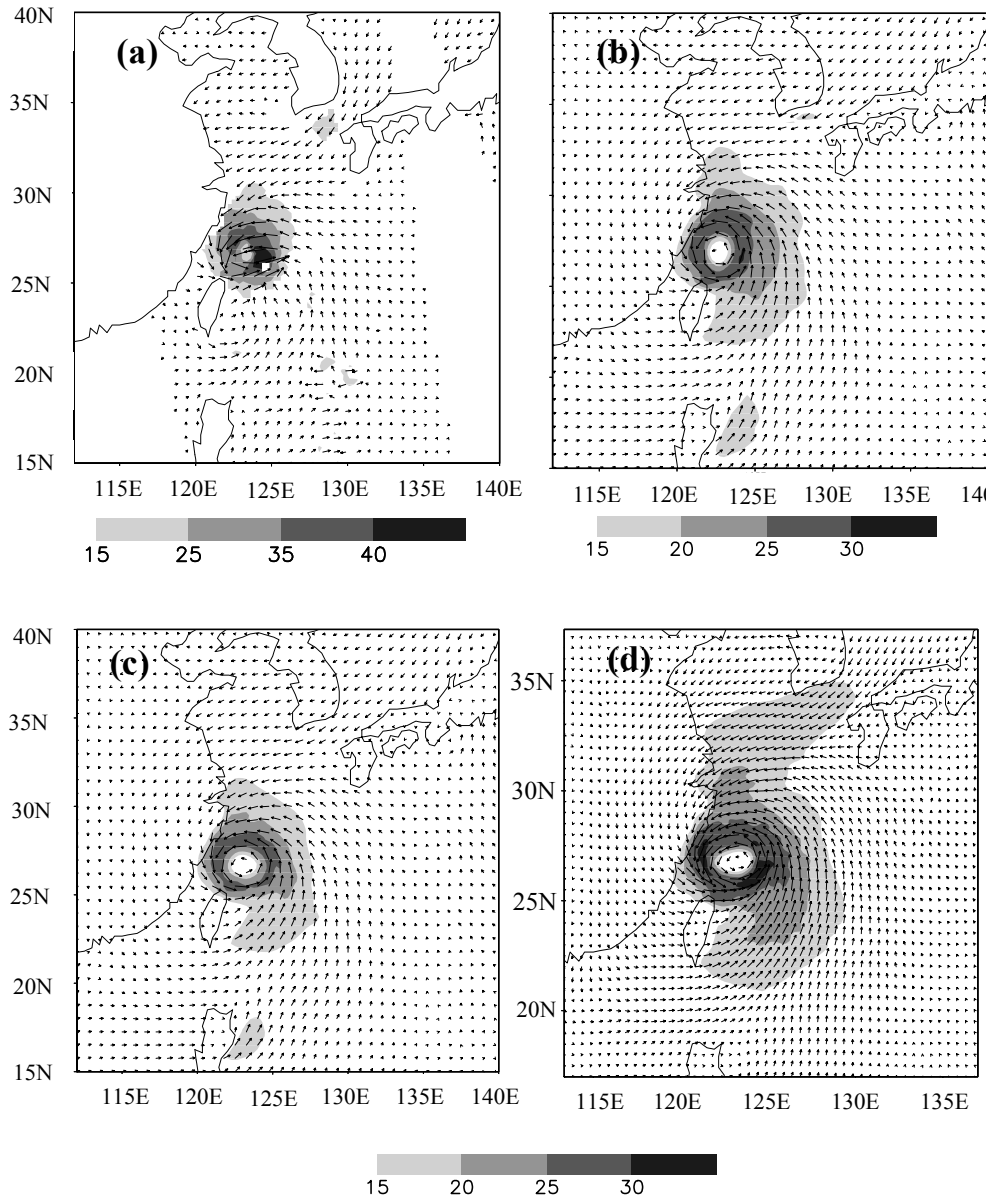

Fig. 4. Surface wind field at 2100 UTC 6 September from (a) QUIKSCAT/NCEP blended wind fields (http://www.ssmi.com), (b) MC2-L, (c) MC2-SST, and (d) MC2-H. (Units: m s^{-1}).

shown in Fig. 6. The potential temperature in the eye is relatively high at the low-level (>365 K), and slightly lower in the mid and upper troposphere with a nearly constant value in the vertical. Compared with MC2-L and MC2-H, MC2-SST has lower potential temperature in the eye and surrounding area. This reduction in warm-moist air in MC2-SST is likely related with the less sensible and latent heat fluxes from the ocean to the typhoon eye, which will be discussed in the following section.

3.4 *Surface latent and sensible heat fluxes*

Spatial distributions of the latent heat flux at integration hours 24, 48, and 72 for the three experiments are shown in Fig. 7. Corresponding sensible heat fluxes are shown in Fig. 8. The latent heat flux, which has already been shown to be a dominant forcing in the development of mesoscale structures in the marine atmospheric boundary layer (MABL) (Warner et al., 1990), has dominant over sensible heat flux during the whole

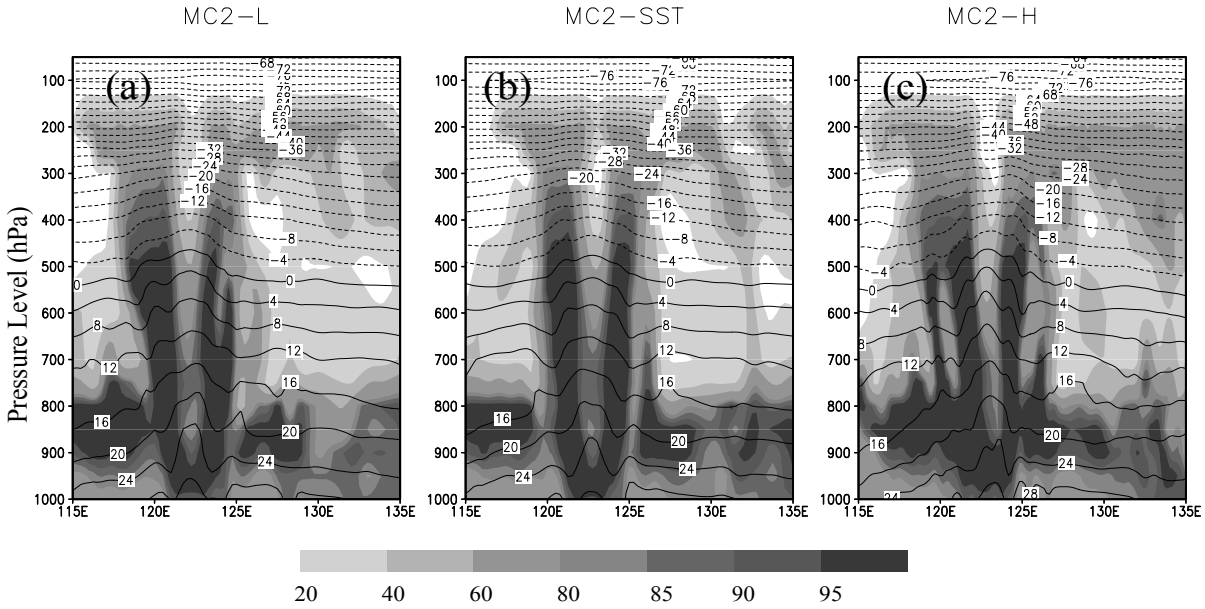

Fig. 5. Vertical cross sections of relative humidity (shaded, unit: %) and air temperature (contours, unit: °C) along the east-west oriented line through the eye of the storm at integration hour 48 for (a) MC2-L, (b) MC2-SST and (c) MC2-H.

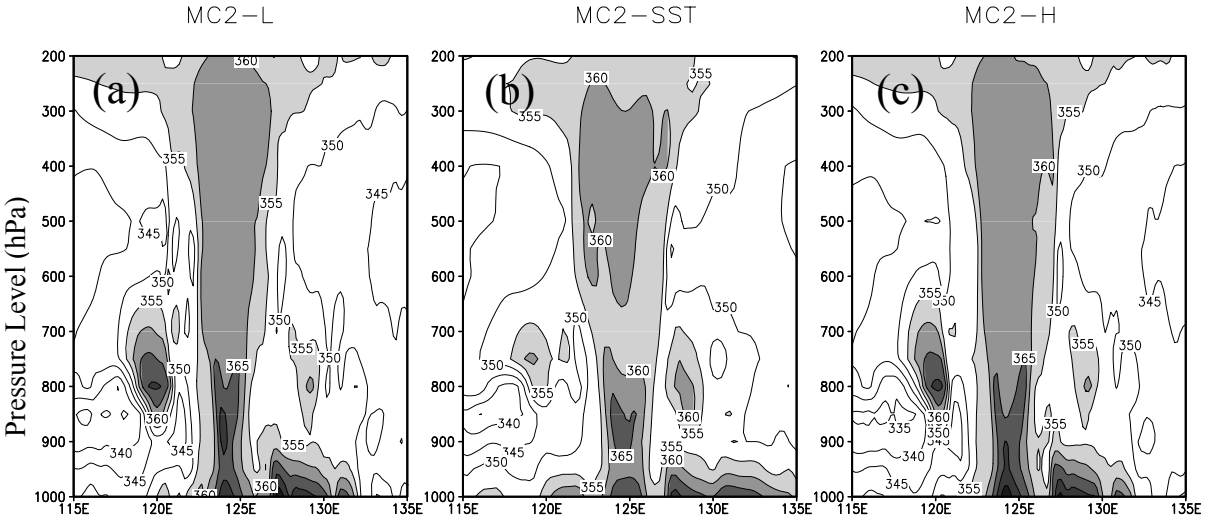

Fig. 6. As in Fig. 5, but for potential temperature (Unit: K). The contour interval is 5 K.

integration stage for the three experiments. The spatial structures of latent and sensible heat fluxes are similar to the low-level wind structure. In the eye region, the underlying ocean provides much less surface flux to the storm due to low wind speeds there. Surrounding the eye, large quantities of surface heat fluxes are emitted from the ocean to the cyclone, because of the high-speed winds. The boundary of the eye is characterized by a high horizontal heat flux gradient. Inside the wall, the high heat fluxes belts are mostly biased to the maximum wind speed belts. The cyclone obtains more surface heat fluxes at 48 h than at 24 h or 72 h, due to the higher wind speed combined with the higher air-sea temperature difference at 48 h (figure not shown).

Less latent heat and sensible heat flux are provided to the cyclone by the underlying ocean in MC2-SST. For example, the maximum latent heat fluxes for MC2-L at 24 h, 48 h and 72 h are 840, 1040, and 950 W m^{-2}, respectively, compared to 640, 780, and 720 W m^{-2} for MC2-SST. The only difference between MC2-L and MC2-SST is the reduced SST field in MC2-SST.

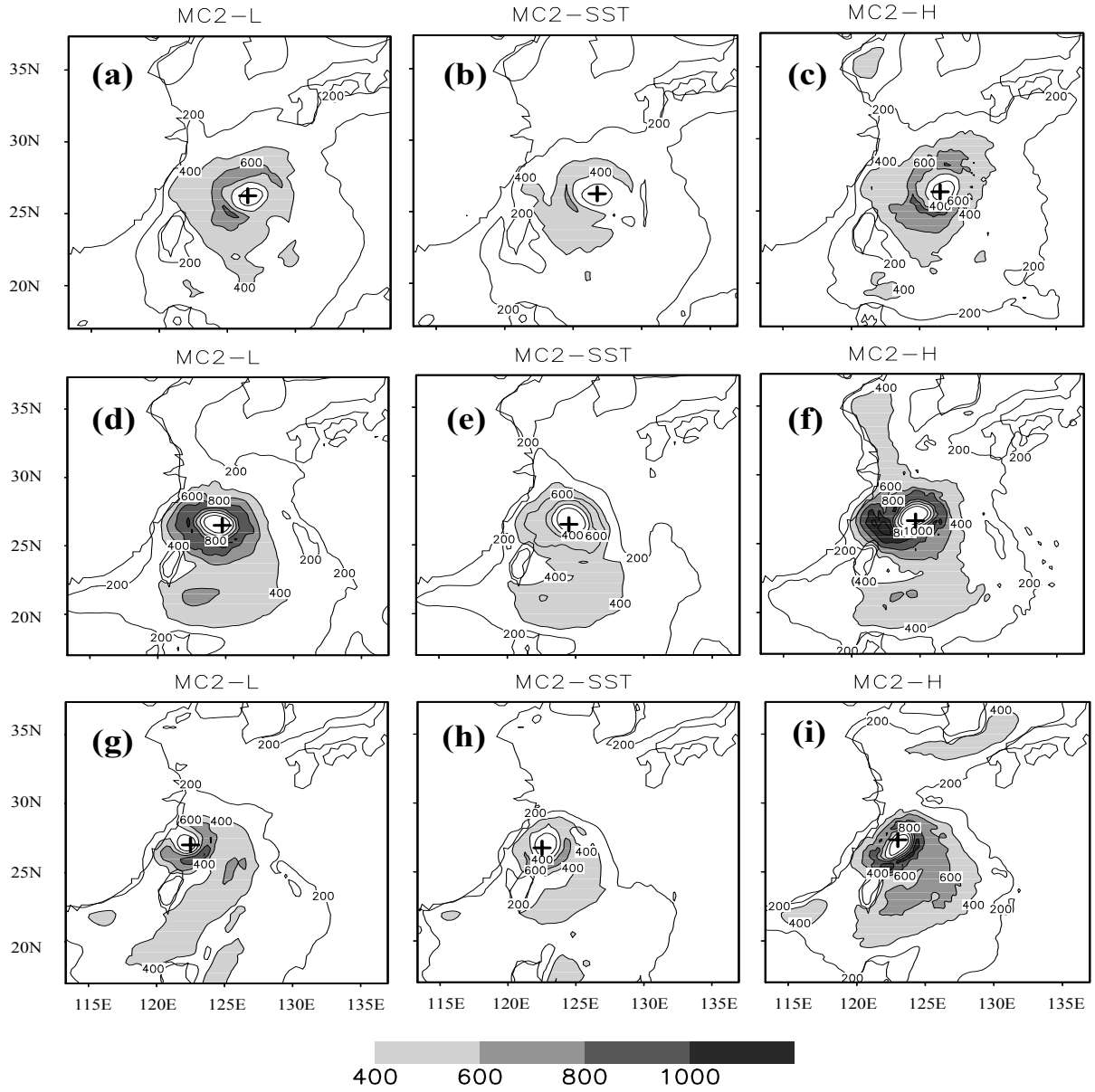

Fig. 7. Latent heat fluxes at 24 h for (a) MC2-L, (b) MC2-SST and (c) MC2-H. Here (d), (e), (f) and (g), (h), (l) are the same as (a), (b), (c), but for 48 h, 72 h respectively. The cross marks in the plots are the cyclone centre. The unit of latent heat flux is W m^{-2}. The contour interval is 200 W m^{-2}.

Therefore, the SST cooling induces less surface heat flux from the ocean to the cyclone, and has a damping effect on the cyclone intensity (see Fig. 3).

By comparison, more surface heat flux is emitted from the ocean surface to the cyclone in MC2-H, than with MC2-L. For example, the maximum latent heat fluxes for MC2-H at 24 h, 48 h and 72 h are 900, 1320, and 1160 W m^{-2}, respectively.

Figure 9 shows the cross sections of 10-m wind, sea-air temperature difference and sea-air specific humidity difference at 2 m, and surface heat fluxes along the east-west oriented line through the eye of the typhoon after integration, for the three experiments. The spatial distributions of surface heat fluxes are mainly decided by the wind structure. In the typhoon eye (near 125°E), the near-zero surface heat fluxes are related to the calm wind. In the wall region, the highest heat fluxes correspond to the strongest wind peak in the wall. At the same time, the sea-air differences in Figs. 9b and 9c are smaller in the eye and larger in the wall, and these are also conducive to the surface heat spatial distributions. It is obvious that, compared with

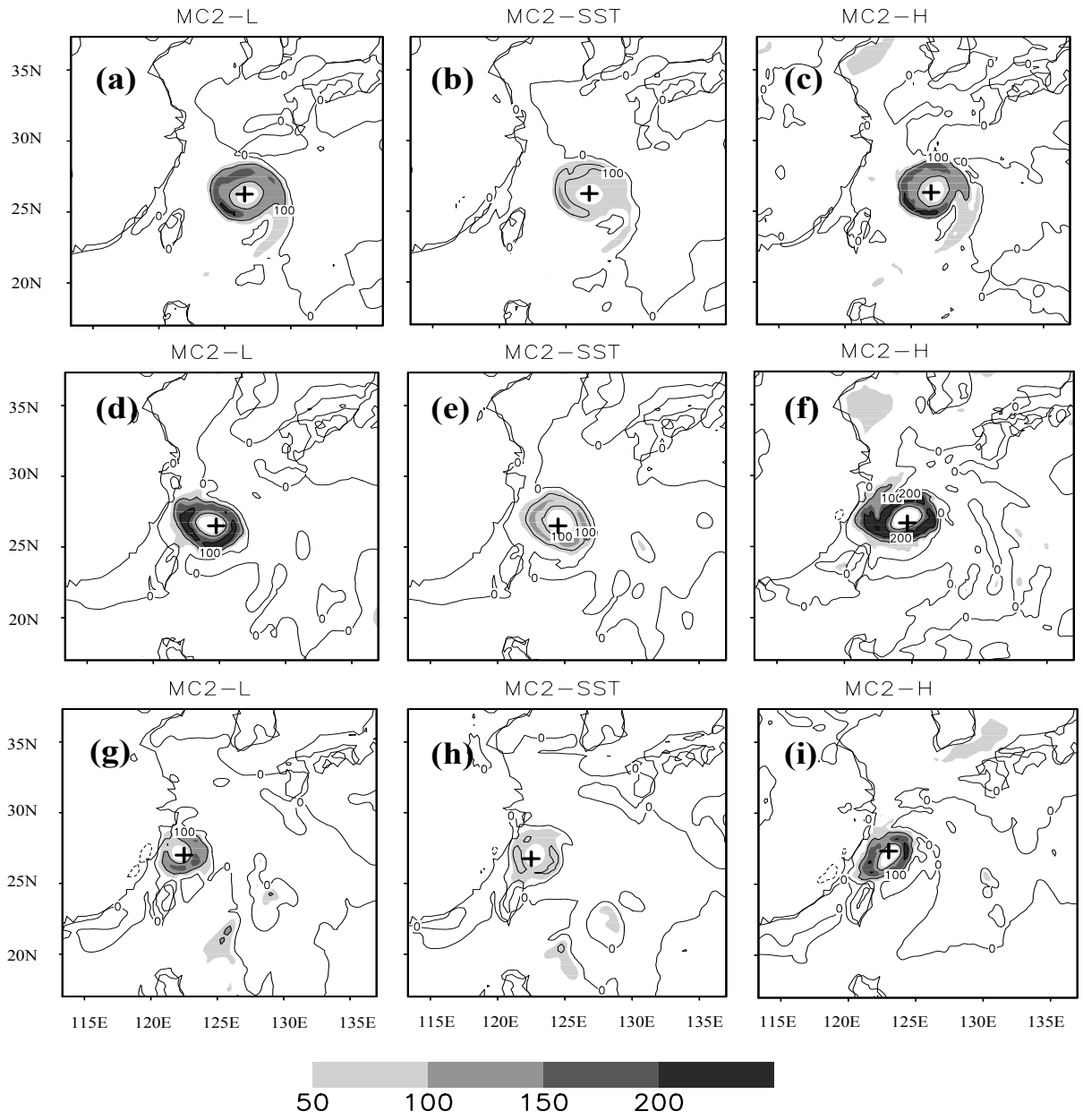

Fig. 8. As in Fig. 7, but for sensible heat flux. The contour interval is 100 W m^{-2}.

MC2-L, the surface heat fluxes provided to the cyclone are lower in MC2-SST due to the weaker surface wind speed and smaller sea-air differences. There is no notable difference between MC2-L and MC2-H for sea-air difference in the wall region in Figs. 9b and 9c. However, MC2-H produces stronger surface winds in the wall than MC2-L, which induces higher surface heat fluxes than MC2-L.

4. Discussion and conclusion

Three experiments are performed in this study using the Canadian MC2 atmospheric model: (1) control run denoted MC2-L, (2) 1°C cooler SST run denoted MC2-SST and (3) finer horizontal resolution run denoted MC2-H. This paper demonstrates that even running at the relatively low resolution of $0.25° \times 0.25°$ in MC2-L, the MC2 model is capable of simulating the development and most of the mesoscale features of typhoon Sinlaku, 2002. These include the rapid deepening, the central low pressure, and the structure of the eye and the eye wall. With the finer horizontal resolution of $(1/6)° \times (1/6)°$, the model produces higher surface wind and a slightly more complex cyclone vertical structure. Another interesting issue is the sensitivity of the typhoon evolution to SST cooling. It is found

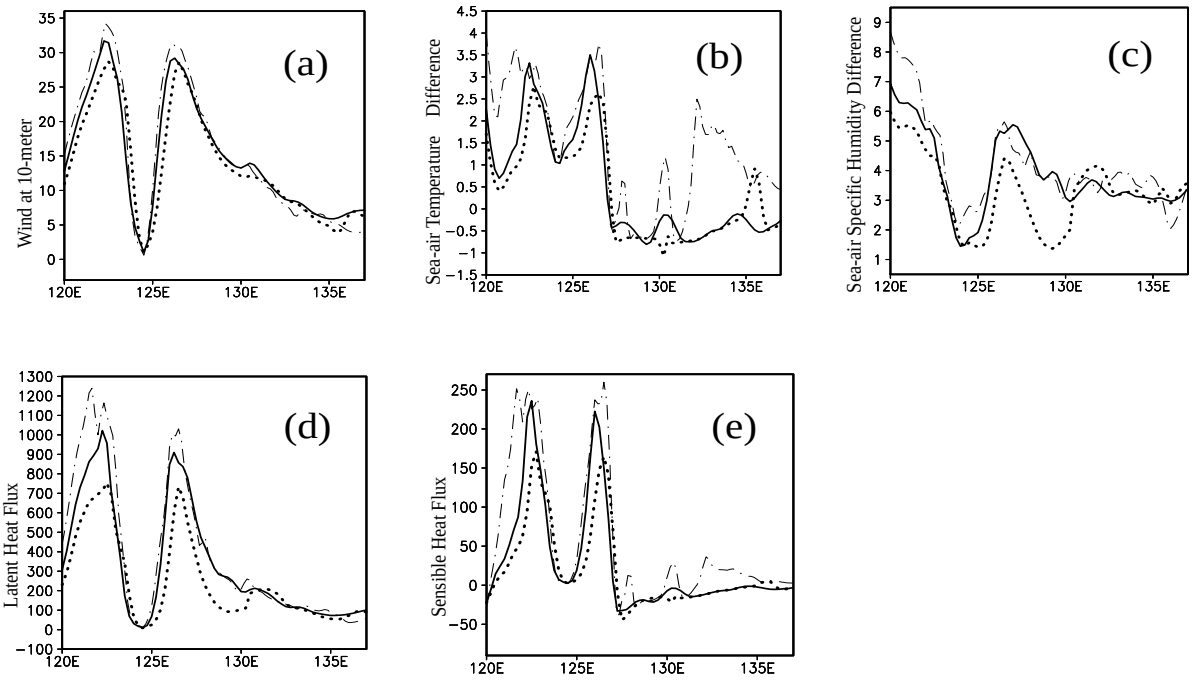

Fig. 9. Cross sections of V_{10} (a, m s^{-1}), sea-air temperature difference (b, °C), sea-air specific humidity difference (c, g kg^{-1}), latent heat flux (d, W m^{-2}) and sensible heat flux (e, W m^{-2}), along the east-west oriented line through the eye of the storm at integration hour 48 for MC2-L (solid line), MC2-SST (dotted line) , and MC2-H (dashed-dotted line).

that surface heat fluxes have a substantial influence on the a slow-moving cyclone throughout its lifecycle. When the SST in the East China coastal ocean becomes 1°C cooler, less surface heat fluxes are provided to the cyclone from the underlying ocean, leading to less warm-moist air inside the cyclone. The cyclone is weakened by 7 hPa at the peak time, and shows a more accurate storm track before and after landfall. A more detailed investigations of the sea-air interactions during cyclone conditions should be performed using a composite atmosphere-ocean coupled model, following the experiments performed by Bender and Ginis (2000).

Acknowledgments. This study was jointly supported by the National Natural Sciences Foundation of China project (Grant No. 40333026), and the Returnee's Science and Technology Activities project 2005. Funding for Dr. William Perrie was provided by the Canadian Panel on Energy Research and Development (PERD), the Natural Sciences and Engineering Research Council of Canada, the Canada Foundation for Climate and Atmospheric Sciences, and Petroleum Reseach Atlantic Canada. The authors thank Dr. John R. Gyakum and Dr. McTaggart-Cowan for their discussions about Canadian MC2. We also thank the two anonymous reviewers for their sound criticism and insightful suggestions, which led to the substantial improvement of this paper.

REFERENCES

Bao, J.-W., J. M. Wilczak, J.-K. Choi, and L. H. Kantha, 2000: Numerical simulations of sea-air interaction under high wind conditions using a coupled model: A study of hurricane development. *Mon. Wea. Rev.*, **128**, 2190–2210.

Bender, M. A., and I. Ginis, 2000: Real-case simulations of hurricane-ocean interaction using a high-resolution coupled model: Effects on hurricane intensity. *Mon. Wea. Rev.*, **128**, 917–946.

Benoit, R., M. Desgagne, P. Pellerin, Y. Chartier, and S. Desjardins, 1997: The Canadian MC2: A semi-implicit semi-Lagrangian wide-band atmospheric model suited for fine-scale process studies and simulation. *Mon. Wea. Rev.*, **125**, 2382–2415.

Chan, J. C. L., Y. Duan, and L. K. Shay, 2001: Tropical cyclone intensity change from a simple ocean-atmosphere coupled model. *J. Atmos. Sci.*, **58**, 154–172.

Chouinard, C., J. Mailhot, and A. Mitchell, 1994: The Canadian Regional Data Assimilation System: Operational and research applications. *Mon. Wea. Rev.*, **122**, 1306–1325.

Emanuel, K. A., 1999: Thermodynamic control of hurricane intensity. *Nature*, **401**, 665–669.

Holland, G. J., Ed., 1993: The Global Guide to Tropical Cyclone Forecasting. WMO/TD-560, World Meteorological Organisation, Geneva, 337pp.

Kain, J. S., and J. M. Fritsch, 1990: A one-dimensional entraining/detraining plume model and its application

in convective parameterization. *J. Atmos. Sci.*, **47**, 2784–2802.

Kain, J. S., and J. M. Fritsch, 1993: Convective parameterization for mesoscale models: The Kain-Fritsch scheme. The representation of cumulus convection in numerical models. *Meteor. Monogr.*, **27**, Amer. Meteor. Soc., 165–170.

Kurihara Y., M. A. Bender, and R. J. Ross, 1993: An initialization scheme of hurricane models by vortex specification. *Mon. Wea. Rev.*, **121**, 2030–2045.

Li Weibiao, 2004: Modeling sea-air fluxes during a western Pacific typhoon: Role of sea spray. *Adv. Atmos. Sci.*, **21**(2), 269–276.

Lord, S. J., 1991: A bogusing system for vortex circulations in the National Meteorological Center Global Forecast Model. Preprints, *19th Conf. on Hurricane and Tropical Meteorology*, F. L. Miami, Amer. Meteor. Soc., 328–330.

Lu Juntian, 2003: Features of weather/climate over China in 2002. *Meteorological Monthly*, **29**(4), 32–36. (in Chinese)

Nagata, Masashi, and Coauthors, 2001: Meeting Summary: Third COMPARE workshop: A model intercomparison experiment of tropical cyclone intensity and track prediction. *Bull. Amer. Meteor. Soc.*, **82**(9), 2007–2020.

McTaggart-Cowan, R., J. R. Gyakum, and M. K. Yau, 2001: Sensitivity testing of extratropical transitions using potential vorticity inversions to modify initial conditions: Hurricane Earl case study. *Mon. Wea. Rev.*, **129**, 1617–1636.

McTaggart-Cowan, R., J. R. Gyakum, and M. K. Yau, 2003: The influence of the downstream state on extratropical transition: Hurricane Earl (1998) case study. *Mon. Wea. Rev.*, **131**, 1910–1929.

Meng Zhiyong, Chen Liangshou, and Xu Xiangde, 2002: Recent progress on tropical cyclone research in China. *Adv. Atmos. Sci.*, **19**(1), 103–109.

Perrie, W., X. Ren, W. Zhang, and Z. Long, 2004: Simulation of extratropical hurricane Gustav using a coupled atmosphere-ocean-sea spray model. *Geophys. Res. Lett.*, **31**, L03110, doi:10.1029/2003GL018571.

Ren Xuejuan, W. Perrie, Zhenxia Long, and J. Gyakum, 2004: Atmosphere-ocean coupled dynamics of cyclones in the midlatitudes. *Mon. Wea. Rev.*, **132**, 2432–2451.

Robert, A., T. Yee, and H. Ritchie, 1985: A semi-Lagrangian and semi-implicit numerical integration scheme for mutilevel atmospheric models. *Mon. Wea. Rev.*, **113**, 388–394.

Warner, T. T., M. N. Lakhtakia, J. D. Doyle, and R. A. Pearson, 1990: Marine atmospheric boundary layer circulations forced by Gulf Stream sea surface temperature gradients. *Mon. Wea. Rev.*, **118**, 309–323.

Wentz, F. J., and Coauthors, 2000: Satellite measurements of sea surface temperature through clouds. *Science*, **288**, 847–850.

Xue, Z., and C. J. Neumann, 1984: Frequency and motion of western North Pacific tropical cyclones. Tech. Memo. NWS NHC 23, NOAA, Washington DC., 80pp.

Zhang, Da-lin, and Xiaoxue Wang, 2003: Dependence of hurricane intensity and structures on vertical resolution and time-step. *Adv. Atmos. Sci.*, **20**(5), 711–725.

Zou Xiaolei, and Qingnong Xiao, 2000: Studies on the initialization and simulation of a mature hurricane using a variational bogus data assimilation scheme. *J. Atmos. Sci.*, **57**, 836–860.